

Non-Hermitian Chiral Heat TransportGuoqiang Xu,^{1,*} Xue Zhou,^{2,*} Ying Li,^{3,4,*} Qitao Cao,⁵ Weijin Chen,¹ Yunfeng Xiao,⁵
Lan Yang,⁶ and Cheng-Wei Qiu^{1,†}¹*Department of Electrical and Computer Engineering, National University of Singapore,
Kent Ridge 117583, Republic of Singapore*²*School of Computer Science and Information Engineering, Chongqing Technology and Business University,
Chongqing 400067, China*³*Interdisciplinary Center for Quantum Information, State Key Laboratory of Extreme Photonics and Instrumentation,
ZJU-Hangzhou Global Scientific and Technological Innovation Center, Zhejiang University,
Hangzhou 310027, China*⁴*International Joint Innovation Center, Key Lab of Advanced Micro/Nano Electronic Devices and Smart Systems of Zhejiang,
The Electromagnetics Academy at Zhejiang University, Zhejiang University, Haining 314400, China*⁵*State Key Laboratory for Mesoscopic Physics and Frontiers Science Center for Nano-optoelectronics,
School of Physics, Peking University 100871, Beijing, China*⁶*Department of Electrical and Systems Engineering, Washington University,
St. Louis, Missouri 63130, USA*

(Received 20 December 2022; accepted 12 April 2023; published 28 June 2023)

Exceptional point (EP) has been captivated as a concept of interpreting eigenvalue degeneracy and eigenstate exchange in non-Hermitian physics. The chirality in the vicinity of EP is intrinsically preserved and usually immune to external bias or perturbation, resulting in the robustness of asymmetric backscattering and directional emission in classical wave fields. Despite recent progress in non-Hermitian thermal diffusion, all state-of-the-art approaches fail to exhibit chiral states or directional robustness in heat transport. Here we report the first discovery of chiral heat transport, which is manifested only in the vicinity of EP but suppressed at the EP of a thermal system. The chiral heat transport demonstrates significant robustness against drastically varying advections and thermal perturbations imposed. Our results reveal the chirality in heat transport process and provide a novel strategy for manipulating mass, charge, and diffusive light.

DOI: [10.1103/PhysRevLett.130.266303](https://doi.org/10.1103/PhysRevLett.130.266303)

The non-Hermitian Hamiltonian has been widely adopted to study open systems in a plethora of domains ranging from electronics [1], photonics [2], to mechanics [3], featured by the coalescence of the eigenvalues and eigenstates at non-Hermitian degeneracies known as exceptional points (EPs). It has led to many exciting findings, including parity-time symmetry [2,3], half-integer quantized invariants [4], and non-Hermitian topological phases [5–7], chiral dynamic encirclings [8–12], Weyl exceptional rings [13–15], and exceptional nexus [16]. Those breakthroughs further empower many technological innovations, such as single mode lasers [17–19], light steering [20], unidirectional invisibility [21], enhanced sensitivity [22,23], and manipulating electromagnetically induced transparency [24]. The underlying chirality observed at the EP holds the key to achieving unidirectional modes and asymmetric backscattering in judiciously engineered whispering-gallery-mode (WGM) resonators [3,17,24–26].

Classical wave fields are conventionally governed by real-eigenvalue Hamiltonians. In contrast, dissipative diffusion has been found to be skew-Hermitian and its Hamiltonian becomes imaginary [27–30]. To mimic a real

space in diffusion, advection is introduced and tailored to achieve the synthetic dimensions. Thus it becomes possible to observe the long-ignored non-Hermiticity and the existence of EP [27], dynamic encircling [28], topological insulating phases [29], and Weyl exceptional ring [30] in thermal diffusion. One might intuitively conclude that the chiral behaviors in thermal diffusion under a pair of inversed-advective configuration on two system boundaries would, consequently, arise, which refers to the property of the temperature field distributions at the systemic intermediate layer that exhibits mirror symmetry and is not superimposable on each other's mirror image. However, those state-of-the-art studies [27–30] only demonstrate that moving temperature progression coincides with the direction of the most dominating advection externally introduced into the thermal systems [Fig. 1(a)]. This has nothing to do with chirality in heat transport, and chiral heat transport is elusive at large.

We realize asymmetric thermal coupling with judiciously imposed thermal perturbations and observe chiral heat transport. Our system holds an EP through the thermal coupling of unbalanced forward and backward advective

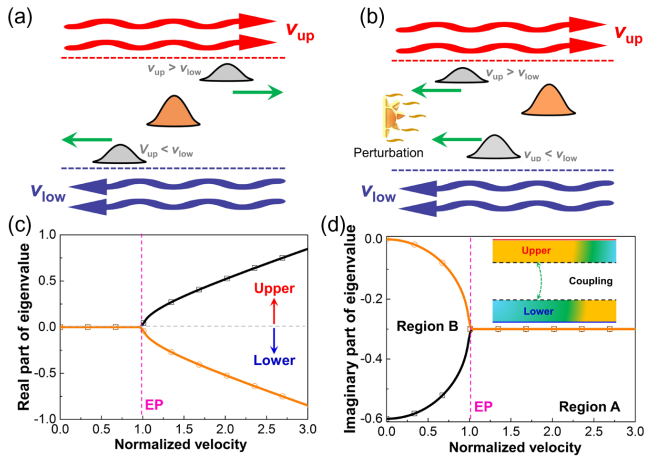


FIG. 1. Schematic of non-Hermitian chiral heat transports. (a) A conventional convective heat transport system without constant thermal perturbations. Two wavelike advection are, respectively, imposed to the upper and lower boundaries. The gray wave packets denote the eigenstates of heat transport under different configurations of the upper and lower advections, and the orange one indicates the initial state without advections. The green arrows indicate the corresponding propagation directions, which are determined by the most dominating advection showcasing different directional biases. (b) The chirality in heat transport under constant thermal perturbations and advections. The eigenstates exhibit robust and same directions. (c) and (d) The real and imaginary eigenvalues of the heat transport in regions A and B, while the thermal distributions (color map) of the upper and lower subparts solely induced by corresponding advection are presented in the inset of (d).

fields. When the thermal system is steered toward approaching the vicinity of EP, we discover the thermal chirality manifested as unidirectional thermal field motion. However, the chiral behavior is found to be suppressed exactly at the EP and far away from the EP, which drastically differs from its photonic counterparts [22–26,31,32]. These distinct chiral and nonchiral heat transports open new paradigms toward realizing handedness in heat and mass diffusion and arbitrary asymmetric thermal manipulations [33–37].

The heat transfer of the proposed fluid system shown in Figs. 2(a) and S1 of the Supplemental Material [38] is

governed by three components, the two countermoving advective fields in the upper and lower subparts ($|v_{up}|$ and $|v_{low}|$ are the velocity magnitude, which are not necessarily balanced), and a global perturbation ($Q_{up/low}$) introduced as a constant conductive heat flux (Supplemental Material, Note 4 [38]). The entire system originates from dissipative diffusion and can be described by the effective Hamiltonian with a global multiplication of “ i ”: $H = i\{(h/\rho_0 c_0 b)\sigma_x + i(k^2 \kappa_0/\rho_0 c_0)\sigma_y - i(k/2)(|v_{up}| + |v_{low}|)\sigma_z - [(k^2 \kappa_0/\rho_0 c_0) + (h/\rho_0 c_0 b)] - i(k/2)(|v_{up}| - |v_{low}|)\}I_{2 \times 2}$, where $\sigma_{x \sim z}$ and $I_{2 \times 2}$ are Pauli matrices and identity matrix, and k denotes the effective wave number for the wavelike temperature. h and b are the convective heat transfer coefficient and the thickness of the components for imposing tailored advections. The imaginary term $[i(k^2 \kappa_0/\rho_0 c_0)]$ along σ_y denotes the constant thermal perturbation. Such a global Hamiltonian as well as the ones in Eqs. S3 and S4 [38] for locally subparts are observed by solving the eigenvalue problems with a wavelike temperature field propagations under the initial temperature field caused by the constant thermal perturbation. They represent the couplings of heat exchanges and the thermal energy caused by the intrinsic conduction, advections, and the input constant thermal perturbation (Supplemental Material, Note 1 [38]). The system holds an EP located at $2[\sqrt{(h/\rho_0 c_0 b)^2 - (k^2 \kappa_0/\rho_0 c_0)^2}] = k|v_{up}| + k|v_{low}| = kv_{EP}$, and v_{EP} denotes the critical value of the sum of velocity amplitudes at the EP. The eigenvalues of the thermal system are presented in Figs. 1(c) and 1(d), where regions A and B are indicated based on v_{EP} at the EP (A for $|v_{up}| + |v_{low}| > v_{EP}$, B for $|v_{up}| + |v_{low}| < v_{EP}$). Under the constant thermal perturbation, only asymmetric and imaginary heat couplings can be observed and further indicates a dominant decay intensity in imaginary space. To study the thermal coupling at the systemic intermediate layer, we first consider the uncoupled limit where only one of the two advective subparts is in contact with the interface [the insets of Fig. 1(d) and Figs. S1 [38]], which can be described by Eqs. (S1)–(S4). The eigenstates of each subpart can be determined:

$$|\psi_{upper}^R\rangle = \begin{bmatrix} 1 \\ -i \left(\pm \frac{1}{2} \sqrt{4 \left(\frac{h}{\rho_0 c_0 b} + \frac{\kappa_0}{\rho_0 c_0} k^2 \right)^2 + (ikv_{up})^2} \right) - \frac{kv_{up}}{2} \\ \frac{h}{\rho_0 c_0 b} + \frac{\kappa_0}{\rho_0 c_0} k^2 \end{bmatrix} = \begin{bmatrix} \psi_1 \\ \psi_{up} \end{bmatrix}, \quad (1)$$

$$|\psi_{\text{lower}}^R\rangle = \left[\frac{-i \left(\pm \frac{1}{2} \sqrt{4 \left(\frac{h}{\rho_0 c_0 b} - \frac{\kappa_0}{\rho_0 c_0} k^2 \right)^2 + (i k v_{\text{low}})^2} \right) + \frac{k v_{\text{low}}}{2}}{\frac{h}{\rho_0 c_0 b} - \frac{\kappa_0}{\rho_0 c_0} k^2} \right] = \begin{bmatrix} \psi_{\text{low}} \\ \psi_3 \end{bmatrix}, \quad (2)$$

where ψ_{up} and ψ_{low} are the local eigenstates of the two interfaces for the systemic intermediate layer [the black dashed-lines of the insets of Fig. 1(d)], and ψ_1 and ψ_3 denote the eigenstates of the upper and lower surfaces of the two subparts [the red and blue solid lines of the insets of Fig. 1(d)]. These local eigenstates stand for the wavelike temperature fields on corresponding surfaces. The solution of the global system can be understood because of further coupling between the two local eigenstates through the systemic intermediate layer [Eq. (S10)]. Then, the criterion for evaluating chirality in the two-mode approximation [25,26] can be expressed by $\alpha = 1 - \min(|\psi_{\text{up}}|, |\psi_{\text{low}}|) / \max(|\psi_{\text{up}}|, |\psi_{\text{low}}|)$. The chirality is suppressed ($\alpha \rightarrow 0$) if $|\psi_{\text{up}}|$ and $|\psi_{\text{low}}|$ are close, and reaches maximum ($\alpha \rightarrow 1$) when they differ significantly. Noting that, the balanced advective fields and absence of thermal perturbation in [27,28] ensure that $\psi_{\text{up}} = -\psi_{\text{low}}^*$, so chirality cannot be observed ($|\psi_{\text{up}}| = |\psi_{\text{low}}|$). Intuitively, the moving direction [27] should follow one of the two countermoving advective fields that has a larger velocity [Fig. 1(a)]. We instead find that the thermal propagation moves along the larger eigenvector and turns robust against external influences [Fig. 1(b)].

We first consider two schemes in region *A* to demonstrate the thermal chirality. The two schemes are selected such that the advective magnitude ($|\psi_{\text{up}}| + |\psi_{\text{low}}|$) is the same, but the forward advection dominates ($|\psi_{\text{up}}| > |\psi_{\text{low}}|$) in scheme 1, while the backward advection dominates ($|\psi_{\text{up}}| < |\psi_{\text{low}}|$) in scheme 2 [Figs. S1(a) and S1(b) [38]]. For the scheme in region *A* with $|\psi_{\text{up}}| > |\psi_{\text{low}}|$ [Fig. S1(a)], the reduction and enhancement in the thermal coupling with thermal perturbation respectively lead to the increased $|\psi_{\text{up}}|$ and suppressed $|\psi_{\text{low}}|$. For scheme 2 with $|\psi_{\text{up}}| < |\psi_{\text{low}}|$, the larger advection $|\psi_{\text{low}}|$ brings a much stronger thermal process to counteract the thermal perturbation from the opposite direction, thus leading to more reduction in $|\psi_{\text{low}}|$ compared with scheme 1 [Fig. S1(b)]. Therefore, the temperature field in the lower subpart is more uniform than that in scheme 1, and the different eigenvectors ($|\psi_{\text{low}}| > |\psi_{\text{up}}|$) as well as the same biased direction can both be retained. In general, the asymmetric heat transport observed in the two subparts as unidirectional motions confirms the significant chirality ($\alpha \rightarrow 1$) of the further coupled state at the intermediate layer of the double-spinning fluid (interface) in region *A*.

The above processes can be also indicated in the eigenvalues [Eq. (S7)] and the eigenvectors [Eq. (S10)] of the global system, whose coalesced imaginary part indicates one decay intensity [Fig. 1(d)], while the split real part provides the nonzero value for drifting the temperature profile [Fig. 1(c)] and exhibiting the biased field distributions [Figs. S1(a) and S1(b) [38]]. The complex eigenvectors of the global system [Eq. (S10)] in region *A* further reveal a nonzero phase deflection in the real space and generate a bias in the temperature field distribution. That is, the chiral heat transport in region *A* is induced by the synergetic effects of the asymmetric heat couplings in imaginary space and the non-zero phase deflection in the real space. We then modify the advective velocities to region *B* where $|v_{\text{up}}| + |v_{\text{low}}| < v_{\text{EP}}$ [Figs. S1(c) and S1(d)]. Since the weak advection in this region has little influence on the conductive processes, $|\psi_{\text{up}}|$ and $|\psi_{\text{low}}|$ are approximately close ($|\psi_{\text{up}}| \approx |\psi_{\text{low}}|$) and their phase differences are simultaneously offset, thus leading to negligible motion in the thermal profiles [green lines in Figs. S1(c) and S1(d)] with the nonchiral ($\alpha \rightarrow 0$) thermal behaviors in region *B*.

Figure 2(a) illustrates a model with a fluidic region to demonstrate the chiral heat transport. We implement a conformal mapping between the schematic model in Cartesian coordinate and the experimental model in cylindrical coordinate (Supplemental Material, Note 14 [38]).

The thermal field propagation and the counteradvection along the parallel direction transform to the azimuth direction [Fig. 2(a)], where the forward and backward motions correspond to the CW and CCW rotations. For observing the chiral behaviors, a consistent heat flow along the *x*-direction is imposed to act as the source for providing the constant thermal perturbation and initial temperature field, and passes through the entire double-spinning fluid region (Fig. S1). Such a constant thermal perturbation maintains constant both in time and space under one heating and one cooling source with constant high and low temperatures along the *x* direction (Fig. S1). The characteristic temperature distributions on the measured lines for clear exhibitions (Supplemental Material, Note 3 [38]) in region *A* are illustrated in [Figs. 2(b)–2(d)]. Here, $|\psi_{\text{up}}|$ driven by CW spinning would be always stronger than $|\psi_{\text{low}}|$ actuated by the CCW spinning as predicted in Fig. S2 [38]. The chirality approaches 1, since the thermal field at the fluid interface moves towards CW

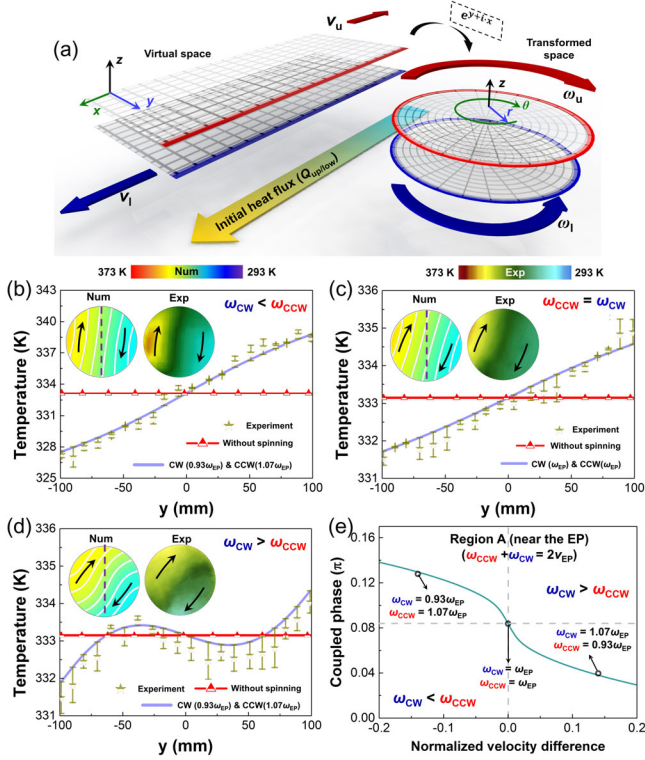


FIG. 2. Chiral heat transport in region A. (a) The transformation between the schematic and experimental models via conformal mapping. The corresponding boundaries between the two spaces are marked by red and blue lines. The counteradvection along the parallel direction in the Cartesian coordinate transform to a pair of CW and CCW spinning on the upper and lower fluidic surfaces. The meshes indicate the spatial distributions of the transformation. (b)–(d) The temperature distributions and thermal profiles of three cases in region A on the measured lines (purple dashed lines), respectively, with different advective configurations. The insets present the calculated (left) and experimental (right) thermal distributions. (e) presents the coupled phase transitions of the final state. The green line is theoretically calculated by considering the additional phase transitions caused by the velocity differences, and the dots refer to those selected cases. The orientations of the coupled phase transitions are robustly towards CW, even though the velocity of CW spinning is smaller.

all the time regardless of the advective magnitudes and thermal perturbation. Some additional phase deflections relative to the case under the same advective magnitudes [(Fig. 2(c)] are also observed under different advective magnitudes [Figs. 2(b) and 2(d)]. These deflections are caused by the velocity difference of the imposed advection as plotted in Fig. 2(e) (Supplemental Material, Note 4 [38]). If the advective strategies of Fig. 2 are inverted as presented in Fig. S1(b), the heat transport would exhibit motion towards CCW direction, indicating the chirality of -1 (Fig. S3). Noted that, the chiral heat transports are suppressed, when the advective velocities are extremely large, i.e., far from the EP in region A [Fig. S1(d)]. In this case, the strong advection enhances the thermal process

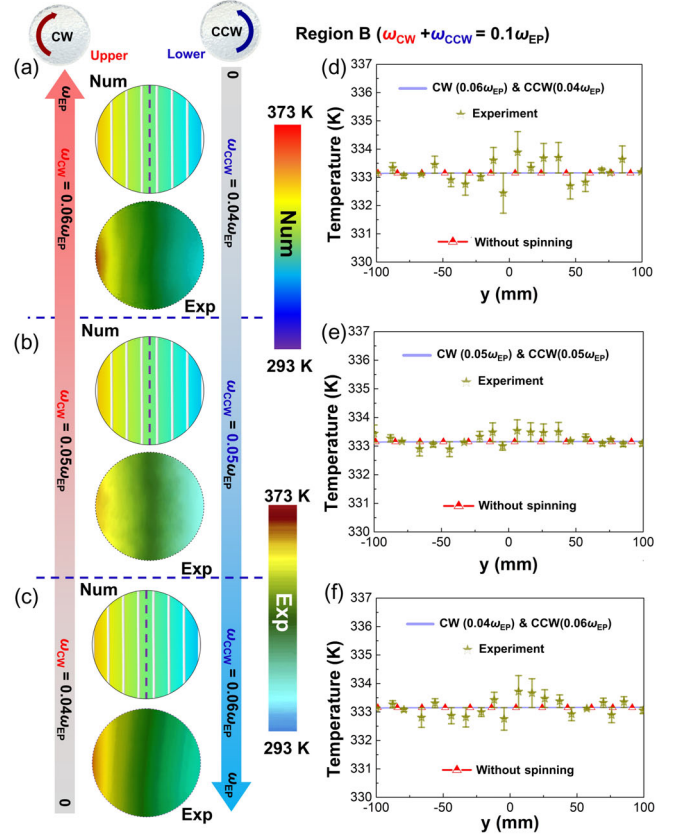


FIG. 3. Nonchiral heat transports in region B. (a)–(c) The temperature distributions in region B under varied advective configurations. The upper and lower images are the simulated and experimental temperatures of these cases. Nonchiral heat transports without biased direction are significant. The purple-dashed lines denote the measured lines. Panels (d)–(f), respectively, denote the characteristic temperature distributions of (a)–(c) on the measured lines (purple dashed lines).

and results in nearly homogeneous temperature field (Supplemental Material, Note 3 [38]).

Further modulating the advective velocities in region B, nonchiral heat transports under varied advective configurations [Figs. 3(a)–3(c)] emerge with unbiased moving directions, which meets well with the theoretical results [Figs. S2(c) and S2(d)]. Conventionally, the intrinsic chirality of EP ensured by symmetric Hamiltonians could enhance the behavior of the chiral state in a photonic system [31]. Nevertheless, the observed state at the EP breaks the expectation in heat transport. When the advective velocities reach the EP, stationary thermal profiles with unbiased moving directions are still significant (Fig. S5), which further suppresses the exhibition of the chirality at the EP (Supplemental Material, Note 5 [38]). Such a vanishing chirality at the EP can be indicated in the global eigenvalues [Figs. 1(c) and 1(d)] and the eigenvector [Eq. (S10)]. When the system reaches the EP, the real part of eigenvalue becomes zero and the imaginary part is

nonzero [Figs. 1(c) and 1(d)]. Besides, the corresponding eigenvectors only possess purely imaginary values without any phase deflections in the real space (Supplemental Material, Note 4 [38]). Both the aspects lead to a non-propagating and purely dissipative decay mode at the EP in the heat transport and result in the absent chirality at the EP in thermal system.

The chiral heat transport provides a distinct mechanism to switch the thermal performance within one fluid. More specifically, the nonchiral or chiral heat transports could act as the control units to be implemented in different areas of a system. Here, we show such a paradigm by integrating the nonchiral and chiral heat transports in one fluid as illustrated in Figs. S6 and S11. The fluid can be divided into three dynamic areas II–IV with separate advective strategies. Thereby, multiple local non-Hermitian systems within the fluid can be created to satisfy the conditions of nonchiral and chiral heat transports. The thermal profiles in different regions give rise to two types of effective conductivities, i.e., the effectively anisotropic conductivities of region A; and the effectively isotropic conductivity of region B (Supplemental Material, Notes 5–9 [38]). These properties pave the way of innovating the thermal metamaterials without any spatial transformations and tailored medium configurations [33]. Here, we adopt three typical thermal functionalities, i.e., cloaking (case 1), transparency (case 2), and twist (case 3), to verify the manipulations induced by nonchiral or chiral heat transport within only one fluid (Supplemental Material, Note 15 [38]). For simplicity, the advective velocities in area III are set to zero. Besides, the advection in area IV is made large in phase A for case 1, and small in phase B for case 2, both away from the EP. For case 3, the advection in region IV is near the EP in phase A.

The nonchiral heat transports in areas IV and unperturbed ambient field distributions are both observed in cases 1 and 2 [Figs. 4(a) and 4(b)]. Because of the selected advection in different areas, a near-zero temperature gradient (cloaking) and a temperature gradient same as the background (transparency) are, respectively, observed in Cases 1 and 2. The different behaviors are governed by the advective strengths of area IV. Besides, both the weak and extreme advection suppress the exhibition of biased directions of thermal field motions. On the contrary, case 3 presents a twisted thermal profile in area IV near the EP in region A. Such a deflected field distribution with biased orientation [Fig. 4(c)] is caused by the effectively anisotropic conductivities. If the spinning directions of the upper and lower fluid fields are reversed, a mirror-symmetric thermal profile can be observed [Fig. 4(d)]. These distributions directly reveal the chiral heat transport in region IV within phase A.

We demonstrate chiral heat transport in a conductive-advective system. Because of the balanced convective effect

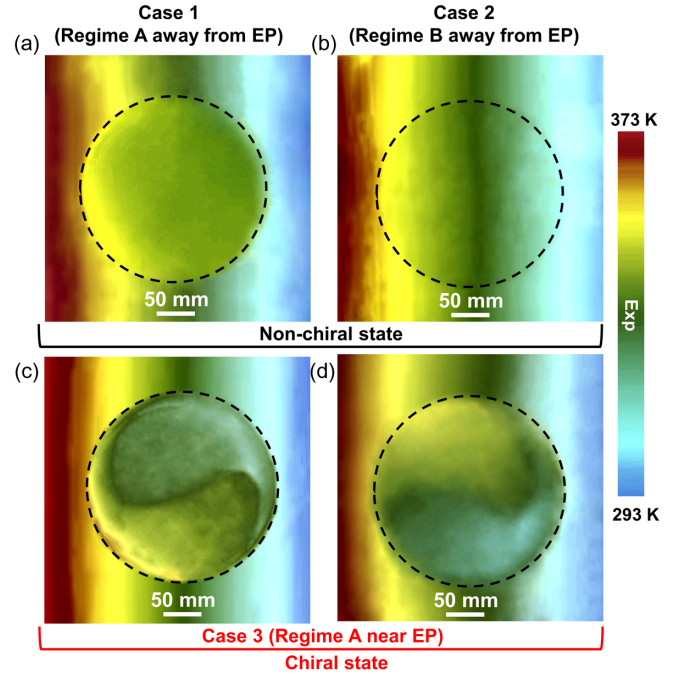


FIG. 4. Thermal manipulations induced by the chiral and nonchiral heat transports. (a)–(d) The captured temperature profiles of cases 1–3, the black-dashed borders indicate the fluidic area. Among them, (a) and (b) present the profiles of cases 1 and 2 induced by the nonchiral heat transports. (c) and (d) illustrate the unidirectional twist profiles of case 3 induced by the chiral states of area IV.

and heat exchange, the chirality at EP is suppressed to render a stationary temperature distribution without directional bias. In parallel, nonchiral temperature distributions are also observed if the advective velocities are far from EP. Only when the advection is off EP and beyond the critical velocity, chiral heat transport emerges, which is robust against the advection and thermal perturbation. Our findings not only reveal the unexpected chiral heat transport, but also present a paradigm of exploring non-Hermitian and unidirectional transport phenomena of heat [33–37], mass [39], fluid flow [40], and charge diffusion [41].

C.-W.Q. acknowledges financial support from the Ministry of Education, Singapore (Grant No. A-8000107-01-00) and the National Research Foundation, Singapore (NRF) under NRF's Medium Sized Centre: Singapore Hybrid-Integrated Next-Generation μ -Electronics (SHINE) Centre funding programme. X. Z. acknowledges the financial support from Chongqing Natural Science Foundation (Grant No. cstc2021jcyj-msxmX0627) and Chongqing Municipal Education Commission (Grant No. KJQN202000829). Y. L. acknowledges the financial support from National Natural Science Foundation of China (Grants No. 92163123 and No. 52250191). Q. C. acknowledges the financial support from National Natural Science Foundation of China (Grants No. 92250302, No. 12174010).

*These authors contributed equally to this work.

†Corresponding author.

chengwei.qiu@nus.edu.sg

- [1] W. Cao, C. Wang, W. Chen, S. Hu, H. Wang, L. Yang, and X. Zhang, Fully integrated parity–time-symmetric electronics, *Nat. Nanotechnol.* **17**, 262 (2022).
- [2] Ş. K. Özdemir, S. Rotter, F. Nori, and L. Yang, Parity–time symmetry and exceptional points in photonics, *Nat. Mater.* **18**, 783 (2019).
- [3] W. Wang, X. Wang, and G. Ma, Non-Hermitian morphing of topological modes, *Nature (London)* **608**, 50 (2022).
- [4] D. Leykam, K. Y. Bliokh, C. Huang, Y. D. Chong, and F. Nori, Edge Modes, Degeneracies, and Topological Numbers in Non-Hermitian Systems, *Phys. Rev. Lett.* **118**, 040401 (2017).
- [5] K. Esaki, M. Sato, K. Hasebe, and M. Kohmoto, Edge states and topological phases in non-Hermitian systems, *Phys. Rev. B* **84**, 205128 (2011).
- [6] S. Yao and Z. Wang, Edge States and Topological Invariants of Non-Hermitian Systems, *Phys. Rev. Lett.* **121**, 086803 (2018).
- [7] K. Takata and M. Notomi, Photonic Topological Insulating Phase Induced Solely by Gain and Loss, *Phys. Rev. Lett.* **121**, 213902 (2018).
- [8] H. Xu, D. Mason, L. Jiang, and J. G. E. Harris, Topological energy transfer in an optomechanical system with exceptional points, *Nature (London)* **537**, 80 (2016).
- [9] J. Doppler, A. A. Mailybaev, J. Böhm, U. Kuhl, A. Girschike, F. Libisch, T. J. Milburn, P. Rabl, N. Moiseyev, and S. Rotter, Dynamically encircling an exceptional point for asymmetric mode switching, *Nature (London)* **537**, 76 (2016).
- [10] J. W. Yoon, Y. Choi, C. Hahn, G. Kim, S. K. Song, K. Y. Yang, J. Y. Lee, Y. Kim, C. S. Lee, J. K. Shin, H. S. Lee, and P. Berini, Time-asymmetric loop around an exceptional point over the full optical communications band, *Nature (London)* **562**, 86 (2018).
- [11] X. L. Zhang, S. Wang, B. Hou, and C. T. Chan, Dynamically Encircling Exceptional Points: In Situ Control of Encircling Loops and the Role of the Starting Point, *Phys. Rev. X* **8**, 021066 (2018).
- [12] X. Zhang, T. Jiang, and C. T. Chan, Dynamically encircling an exceptional point in anti-parity-time symmetric systems: Asymmetric mode switching for symmetry-broken modes, *Light* **8**, 88 (2019).
- [13] A. Cerjan, S. Huang, M. Wang, K. P. Chen, Y. Chong, and M. C. Rechtsman, Experimental realization of a Weyl exceptional ring, *Nat. Photonics* **13**, 623 (2019).
- [14] Y. Xu, S. T. Wang, and L. M. Duan, Weyl Exceptional Rings in a Three-Dimensional Dissipative Cold Atomic Gas, *Phys. Rev. Lett.* **118**, 045701 (2017).
- [15] A. Cerjan, M. Xiao, L. Yuan, and S. Fan, Effects of non-Hermitian perturbations on Weyl hamiltonians with arbitrary topological charges, *Phys. Rev. B* **97**, 075128 (2018).
- [16] W. Tang, X. Jiang, K. Ding, Y. X. Xiao, Z.-Q. Zhang, C. T. Chan, and G. Ma, Exceptional nexus with a hybrid topological invariant, *Science* **370**, 1077 (2020).
- [17] B. Peng, S. K. Özdemir, S. Rotter, H. Yilmaz, M. Liertzer, F. Monifi, C. M. Bender, F. Nori, and L. Yang, Loss-induced suppression and revival of lasing, *Science* **346**, 328 (2014).
- [18] L. Feng, Z. J. Wong, R. M. Ma, Y. Wang, and X. Zhang, Single-mode laser by parity-time symmetry breaking, *Science* **346**, 972 (2014).
- [19] H. Hodaei, M. A. Miri, M. Heinrich, D. N. Christodoulides, and M. Khajavikhan, Parity-time-symmetric microring lasers, *Science* **346**, 975 (2014).
- [20] H. Zhao, X. Qiao, T. Wu, B. Midya, S. Longhi, and L. Feng, Non-Hermitian topological light steering, *Science* **365**, 1163 (2019).
- [21] Z. Lin, H. Ramezani, T. Eichelkraut, T. Kottos, H. Cao, and D. N. Christodoulides, Unidirectional Invisibility Induced by PT-Symmetric Periodic Structures, *Phys. Rev. Lett.* **106**, 213901 (2011).
- [22] W. Chen, Ş. Kaya Özdemir, G. Zhao, J. Wiersig, and L. Yang, Exceptional points enhance sensing in an optical microcavity, *Nature (London)* **548**, 192 (2017).
- [23] H. Hodaei, A. U. Hassan, S. Wittek, H. Garcia-Gracia, R. El-Ganainy, D. N. Christodoulides, and M. Khajavikhan, Enhanced sensitivity at higher-order exceptional points, *Nature (London)* **548**, 187 (2017).
- [24] C. Wang, X. Jiang, G. Zhao, M. Zhang, C. W. Hsu, B. Peng, A. D. Stone, L. Jiang, and L. Yang, Electromagnetically induced transparency at a chiral exceptional point, *Nat. Phys.* **16**, 334 (2020).
- [25] B. Peng, Ş. Özdemir, M. Liertzer, W. Chen, J. Kramer, H. Yilmaz, J. Wiersig, S. Rotter, and L. Yang, Chiral modes and directional lasing at exceptional points, *Proc. Natl. Acad. Sci. U.S.A.* **113**, 6845 (2016).
- [26] B. Peng, S. K. Özdemir, F. Lei, F. Monifi, M. Gianfreda, G. L. Long, S. Fan, F. Nori, C. M. Bender, and L. Yang, Parity-time-symmetric whispering-gallery microcavities, *Nat. Phys.* **10**, 394 (2014).
- [27] Y. Li, Y. G. Peng, L. Han, M. A. Miri, W. Li, M. Xiao, X. F. Zhu, J. Zhao, A. Alù, S. Fan, and C.-W. Qiu, Anti-parity-time symmetry in diffusive systems, *Science* **364**, 170 (2019).
- [28] G. Xu, Y. Li, W. Li, S. Fan, and C.-W. Qiu, Configurable Phase Transitions in Topological Thermal Material, *Phys. Rev. Lett.* **127**, 105901 (2021).
- [29] G. Xu, Y. Yang, X. Zhou, H. Chen, H. Alu, and C.-W. Qiu, Diffusive topological transport in spatiotemporal thermal lattices, *Nat. Phys.* **18**, 450 (2022).
- [30] G. Xu, W. Li, X. Zhou, H. Li, Y. Li, S. Fan, S. Zhang, D. N. Christodoulides, and C.-W. Qiu, Observation of Weyl exceptional rings in thermal diffusion, *Proc. Natl. Acad. Sci. U.S.A.* **119**, e2110018119 (2022).
- [31] W. D. Heiss and H. L. Harney, The chirality of exceptional points, *Eur. Phys. J. D* **17**, 149 (2001).
- [32] H. Nasari, G. Lopez-Galimiche, H. E. Lopez-Aviles, A. Schumer, A. U. Hassan, Q. Zhong, S. Rotter, S. LiKamWa, D. N. Christodoulides, and M. Khajavikhan, Observation of chiral state transfer without encircling an exceptional point, *Nature (London)* **605**, 256 (2022).
- [33] Y. Li, W. Li, T. Han, X. Zheng, J. Li, B. Li, S. Fan, and C. W. Qiu, Transforming heat transfer with thermal metamaterials and devices, *Nat. Rev. Mater.* **6**, 488 (2021).
- [34] R. Ju, G. Xu, L. Xu, M. Qi, D. Wang, H. Chen, C.-W. Qiu, and Y. Li, Convective thermal metamaterials: Exploring high-efficiency, directional, and wave-like heat transfer, *Adv. Mater.* 2209123 (2022), [10.1002/adma.202209123](https://doi.org/10.1002/adma.202209123).

- [35] T. Han, X. Bai, D. Gao, J. T. L. Thong, B. Li, and C.-W. Qiu, Experimental Demonstration of a Bilayer Thermal Cloak, *Phys. Rev. Lett.* **112**, 054302 (2014).
- [36] G. Xu, K. Dong, Y. Li, H. Li, K. Liu, L. Li, J. Wu, and C.-W. Qiu, Tunable analog thermal material, *Nat. Commun.* **11**, 6028 (2020).
- [37] J. Guo, G. Xu, D. Tian, Z. Qu, and C.-W. Qiu, Passive ultra-conductive thermal metamaterials, *Adv. Mater.* **34**, 2200329 (2022).
- [38] See Supplemental Material at <http://link.aps.org/supplemental/10.1103/PhysRevLett.130.266303> for the details of realizing the non-Hermitian chiral heat transport and the potential applications on innovating the conventional thermal metadevices.
- [39] A. D. Poletayev, J. A. Dawson, M. S. Islam, and A. M. Lindenberg, Defect-driven anomalous transport in fast-ion conducting solid electrolytes, *Nat. Mater.* **21**, 1066 (2022).
- [40] J. Li, X. Zhou, J. Li, L. Che, J. Yao, G. Mchale, M. K. Chaudhury, and Z. Wang, Topological liquid diode, *Sci. Adv.* **3**, 3530 (2017).
- [41] P. Song, C.-H. Hsu, G. Vignale, M. Zhao, J. Liu, Y. Deng, W. Fu, Y. Liu, Y. Zhang, H. Lin, V. M. Pereira, and K. P. Loh, Coexistence of large conventional and planar spin Hall effect with long spin diffusion length in a low-symmetry semimetal at room temperature, *Nat. Mater.* **19**, 292 (2020).
- [42] H. Nasari, G. Lopez-Galmiche, H. E. Lopez-Aviles, A. Schumer, A. U. Hassan, Q. Zhong, S. Rotter, P. LiKamWa, D. N. Christodoulides, and M. Khajavikhan, Observation of chiral state transfer without encircling an exceptional point, *Nature (London)* **605**, 256 (2022).